# Ultrafast charge transfer through *p*-oligo(phenylene) bridges: effect of nonequilibrium vibrations

**Christophe Bauer**[1,2,*], **Joël Teuscher**[1,2], **Serge Pelet**[1,2], **Bernard Wenger**[1,2], **Pierre Bonhôte'**[2], **Mohammad K. Nazeeruddin**[2], **Shaik M. Zakeeruddin**[2], **Pascal Comte'**[2], **Michael Grätzel**[2] **and Jacques-Edouard Moser**[1,*]

[1]Photochemical Dynamics Group, [2]Laboratory of Photonics and Interfaces, Basic Sciences, Swiss Federal School of Technology of Lausanne, Lausanne, Switzerland

**Electron transfers (ET) between a donor (D) and an acceptor (A) through a molecular bridge (B) are of great importance in biological systems, molecular electronics and molecular based light-energy conversion systems. Here, the back and the forward electron transfer rates have been measured by femtosecond and nanosecond spectroscopy in a heterogeneous donor–bridge–acceptor (D–B–A) system, where D = ruthenium terpyridine complex, B = *p*-oligo(phenylene) and A = $TiO_2$. The forward ET rate (from 0.85 to 3.7 ps$^{-1}$) is faster than the nonequilibrium vibrations relaxation rate of the hot $^3$MLCT (metal-to-ligand charge transfer) state of the donor (12 ps$^{-1}$ in solution). The back ET occurs on the microsecond time scale. Regarding the distance dependence behaviour, damping factors 0.16 and 0.47 Å$^{-1}$ of the forward and the back ET respectively are obtained. These results confirm that the damping factor is not only linked to the nature of the molecular bridge but to the full D–B–A system. This unusual low damping factor observed for the forward ET is attributed to a decrease of the tunnelling energy gap ΔE, which is induced by the nonequilibrium vibrations at the donor–bridge interface. This enhanced electron transmission is briefly discussed within the concept of a nonequilibrium polaron relaxation towards the dissipative acceptor. In this case, the dissipation of the excess vibrational energy and the electron transfer occur in a synchronized cooperative way.**

**Keywords.** Cooperative effect, molecular electronics, nonlinear phenomena, nonequilibrium phenomena, synchronization, vibronic coupling.

ELECTRON TRANSFER (ET) processes between an electron donor (D) and acceptor (A) separated by a molecular bridge (B), the so-called D–B–A systems, are ubiquitous in biological systems[1–6]. Originally, the studies of electron transport in D–B–A systems began with biological systems with the goal of understanding the mechanisms of the efficient energy flows through proteins or DNA at the molecular level[7–10]. Recently, D–B–A systems have gained much interest due to the emergence of important potential applications. Indeed, a key element for the design and the development of molecular electronics[11–13] and molecular based light-energy conversion systems[14–16] concerns a deeper and global understanding of the factors governing the molecular conductivity. A better knowledge of the relation between the molecular structure and the electron transfer properties of the molecular bridge as well as the physics underlying the charge transport may give new interesting directions for the development of bio-inspired opto-electronic devices.

Among the current open issues on charge transfer through molecular bridges, there is growing interest on the role of molecular vibrations on the electron transmission properties. These vibronic effects may lead to intriguing phenomena such as hysteresis, bistability or negative differential resistance. The consequences of the coupling between tunnelling electrons and molecular vibrations are of crucial importance in molecular bridges due to the following reasons: (i) the current flow can generate local heating with subsequent device degradations, (ii) the vibrational energy may be harnessed to enhance the electron transmission properties of the bridge and (iii) the energetic and dynamical interplay between the electronic and nuclear degrees of freedom may lead to the emergence of complex behaviours.

Earlier studies on the charge transport properties indicate that the current displays an exponential dependence with the molecular bridge length according to the expression $I = I_0 \exp(-\beta l)$, where $l$ is the length of the molecular bridge and $\beta$ the so-called damping factor. In general, the damping factor $\beta$ depends on the degree of conjugation of the molecular bridge and increases from 0.1 Å$^{-1}$ in highly conjugated molecules such as oligo(phenylene-ethynylene) (OPE) to 1 Å$^{-1}$ in alkyl bridges.

Previously, the distance dependence of charge transport properties of *p*-oligo(phenylene) bridges was studied with

*For correspondence. (e-mail: christophe.bauer@epfl.ch; je.moser@epfl.ch)

self-assembled monolayers by current measurements[17–19], time-resolved spectroscopy in solution[20–22] and quantum conductance of single *p*-oligo(phenylene)[23]. All these studies report a charge transport by coherent tunnelling illustrating the intimate relationship between the ET rates and conductance through molecules[24].

The objective of the present study is to gain information on electron transmission properties of *p*-oligo(phenylene) bridges on ultrafast time scale by femtosecond pump–probe transient absorption spectroscopy. For this purpose, we have assembled a heterogeneous D–B–A system, where D = ruthenium terpyridine complex, B = *p*-oligo(phenylene) and A = TiO$_2$ (see Figure 1). These heterogeneous D–B–A systems have specific properties. Indeed, FET rates in these heterogeneous D–B–A systems are expected to be two orders of magnitude faster with respect to homogeneous D–B–A systems[20–22]. This is due to the high density of empty electronic states of the TiO$_2$ conduction band, which leads to a giant electronic coupling between the donor and the acceptor. As an important consequence, ET rate can be compared to the rate of nonequilibrium vibrations relaxation. Compared to homogeneous D–B–A systems, where the molecular bridge is coupled to discrete electronic state of the acceptor, here the phenylene bridges are connected to a quasi-continuum of states of the TiO$_2$ substrate. In addition, as the acceptor used in the present D–B–A system is a solid, it can act as a heat bath via phonon emission upon the relaxation of nonequilibrium molecular vibrations. Very recently, studies on the distance dependence were also made by time-resolved spectroscopy with a metal oxide semiconductor as the acceptor. For example, ET rates have been measured in a series of Re complexes with alkyl chains adsorbed onto TiO$_2$ and SnO$_2$[25–28], perylene-based tripodal sensitizers[29,30] and *p*-OPE bridges[31].

The molecules used here to build the D–B–A systems are (C$_4$H$_9$)$_4$N[2,2′:6′,2″-terpyridine-4′-phosphonate(NCS)$_3$-Ru] (*P*$_0$), (C$_4$H$_9$)$_4$N[2,2′:6′,2″-terpyridine-4′-phenyl-4″-phosphonate(NCS)$_3$Ru] (*P*$_1$) and (C$_4$H$_9$)$_4$N[2,2′:6′,2″-

terpyridine-4′-diphenyl-4″-phosphonate(NCS)$_3$Ru] (*P*$_2$). The choice for these ruthenium terpyridine dyes has been motivated by their well characterized spectral properties. In contrast to Ru polypyridyl complexes, Ru terpyridine dyes exhibit a clear spectral separation between the excited and the oxidized state, which allows unambiguous measurements of the electron transfer rates. Due to their rigidity, the *p*-oligo(phenylene) bridges allows to find the distance between the donor and the acceptor in contrast to flexible bridges such as alkyl chains. Finally, *p*-oligo(phenylene) bridges are a class of rigid molecular bridges with the highest damping factor, due to the moderate conjugation of *p*-oligo(phenylene) bridges originating from the torsion angle between the phenyl units. This is advantageous to observe changes in the damping factor. The attachment of the donor–bridge system onto the TiO$_2$ surface is identical for the three D–B–A systems and occurs via the phosphonate groups with a bidentate binuclear mode, i.e. two oxygen atoms of phosphonate group are linked to two surface titanium atoms[32].

The topic of electron transfer dynamics in dye–semiconductor nanosystems is well documented[33–43]. The electron transfer processes occurring in these systems can be summarized as follows: upon visible light absorption by the adsorbed dye molecule (eq. (1)), an electron injection occurs from the dye excited state into the conduction band of TiO$_2$ (eq. (2)). The long-lived charge separated state is followed by a recombination (eq. (3)).

$$D–B–TiO_2 + h\nu \rightarrow D^*–B–TiO_2 \qquad (1)$$

$$D^*–B–TiO_2 \rightarrow D^+–B–TiO_2\ (e^-) \qquad (2)$$

$$D^+–B–TiO_2\ (e^-) \rightarrow D–B–TiO_2. \qquad (3)$$

To determine the dynamics of the forward and the back electron transfer processes between D and A the Ru terpyridine complex and the TiO$_2$, we first measure the differential transient absorption spectra of the excited and the oxidized state of the Ru terpyridine species. From these spectra, we choose an appropriate wavelength allowing to probe the temporal evolution of the dye excited state as well as the formation of the charge separated state (eq. (2)). Using this approach, we can determine the dynamics of forward electron transfer from the Ru terpyridine complex to the TiO$_2$ surface (eq. (2)) as well as the back electron transfer (eq. (3)) as a function of the bridge length.

## Experimental methods

### Dye synthesis

Details on molecular bridges synthesis and characterization, available as supporting information, can be obtained from the authors.
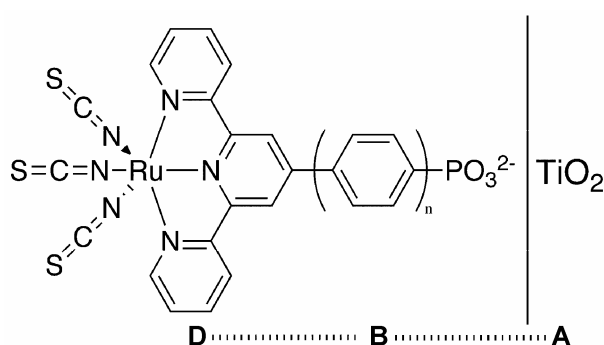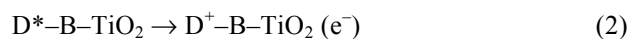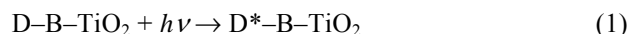


**Figure 1.** Structure of the D–B–A systems with (D) the ruthenium terpyridine dye as a sensitizer chromophore (B) the oligophenylene bridge and (A) the TiO$_2$ semiconductor as an acceptor. The distances between the donor and the acceptor in *P*$_0$, *P*$_1$ and *P*$_2$ systems are 9, 13.4 and 17.8 Å respectively.

## Samples preparation

The three D–B–A systems were prepared under identical conditions. Nanocrystalline $TiO_2$ films (8 μm thick) were soaked for 16 h in the dye solutions (0.3 mM in ethanol). The resulting dye-sensitized $TiO_2$ films were carefully washed with ethanol and dried before taking the time-resolved measurements.

## UV-Vis spectroscopy

Steady-state absorption was carried out on a HP-8353 spectrophotometer (Hewlett–Packard).

## Femtosecond spectroscopy

The femtosecond laser system has been described else-where[36]. Briefly, the femtosecond transient absorption set-up features a Ti : sapphire-amplified femtosecond laser with a repetition rate of 1 kHz, a fundamental wavelength at 775 nm, a pulse width of 120 fs and an energy of 1 mJ per pulse. The output beam was split into three parts for pumping two double-stage noncolinear optical parametric amplifiers (NOPAs) and to produce a white light continuum in a 2 mm thick sapphire plate. The signal from the detector was connected to a lock-in amplifier tuned at 220 Hz by a chopper modulating the pump beam.

## Flash photolysis

Nanosecond flash photolysis experiments were carried out with a Q-switched Nd : YAG laser set-up with 5 ns pulses at a repetition rate of 30 Hz. The third harmonic (355 nm) of the fundamental wavelength (1064 nm) was sent into an optical parameteric oscillator (OPO) to tune the excitation wavelength. The absorbance changes were measured using a Xe lamp and a fast photomultiplier after passing through a monochromator.

## Results

### Electronic absorption spectra

Figure 2 shows the electronic absorption spectra of $P_0$, $P_1$ and $P_2$ in ethanolic solutions. All the three dyes exhibit comparable spectra in the visible range. The bands at 570, 520 and 370 nm are linked to the lowest metal to ligand electronic transitions (MLCT), whereas bands at 310 and 264 nm are due to $\pi$–$\pi$* transitions in the terpyridine rings. The similar spectra of the three dyes in the visible range indicate that the phenylene bridges in $P_1$ and $P_2$ do not participate in the MLCT transitions.

## Excited state lifetime in solution

The differential transient absorption spectra of $P_0^*$ were identified by flash photolysis spectroscopy. Figure 3 shows the transient spectrum of $P_0$ in methoxy proprionitrile solution recorded 30 ns after pulsed excitation at 520 nm. The absorption maximum observed at 570 nm is attributed to the excited state. The absence of a bleach of the excited state of the Ru terpyridine chromophore is rationalized by the higher extinction coefficient of the terpyridine radical anion compared to the ground state[44,45]. The excited state of $P_0$ has a lifetime of 34 ns in aerated methoxy proprionitrile as measured at 570 nm by flash photolysis (see inset of Figure 3).
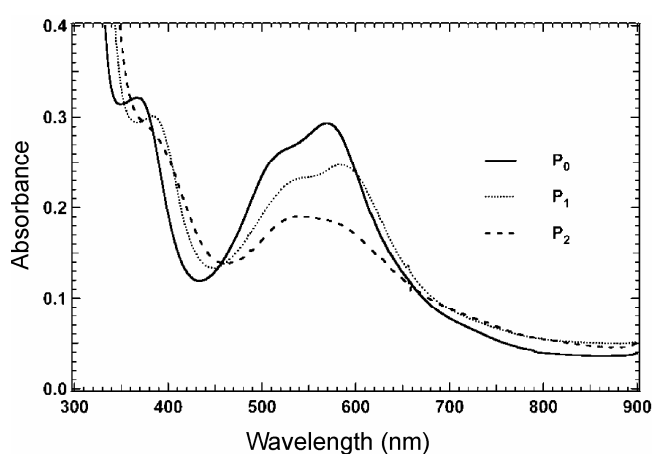


**Figure 2.** Absorption spectra of $P_0$, $P_1$ and $P_2$ systems in ethanolic solutions.
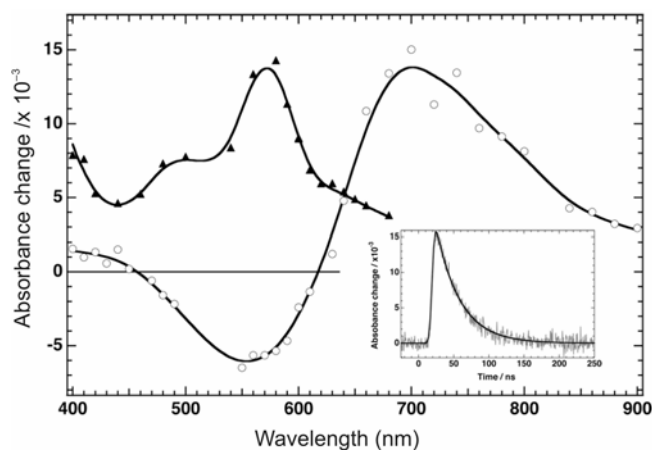


**Figure 3.** Differential transient absorption spectra of $P_0$ in 3-methoxy proprionitrile (triangles) recorded 30 ns after pulsed excitation at 520 nm. Differential transient absorption spectra of $P_0$ adsorbed onto $TiO_2$ surface (circles) recorded 1 μs after pulsed excitation at 520 nm. Inset: Transient absorption data recorded at 570 nm after pulsed excitation at 520 nm. The trace can be well fitted with a single exponential function convoluted with a Gaussian instrument response (full width at half maximum (FWHM) = 7.1 ns).

### Transient spectra of $P_0^+$

Figure 3 shows the differential absorption spectra recorded 1 µs after laser pulsed excitation at 520 nm. In contrast to spectra of $P_0^*$ obtained in solution, a bleach is observed between 450 and 620 nm, which is attributed to the ground state depletion whereas an absorption is observed from 620 to 900 nm due to the spectral signature of $P_0^+$ and injected electrons into the TiO$_2$ nanoparticles. Indeed, the spectrum of the oxidized state of the carboxylate analogue of $P_0$ obtained by spectroelectrochemical measurements exhibits a bleach and an absorption at 610 and 760 nm respectively[45]. Therefore, these spectra are attributed to the charge-separated state (eq. (2)). Another indication for the assignment of these spectra to the charge-separated state comes from the lifetime of the bleach at 600 nm, which falls in the microsecond regime.

### Ultrafast dynamics of the donor $P_0$ in solution

Figure 4 shows the transient absorption data obtained by probing the donor excited state at 570 nm in ethanolic solutions. At this probe wavelength, the thermalized $^3$MLCT state is monitored. The signal exhibits a fast rise within the instrument response time followed by a slower rise until a plateau is reached. The non-instantaneous rise indicates that the transient absorption spectrum of the thermalized $^3$MLCT state is not fully developed within the first tens of picoseconds. The data can be well fitted with a bi-exponential function. The fast component occurs within the instrument response (54%) followed by a slow component with a time constant of 12 ps (46%). The fast component is attributed to the formation of the hot $^3$MLCT state after internal system crossing[46]. On the basis of ultrafast photophysics of metal polypyridine
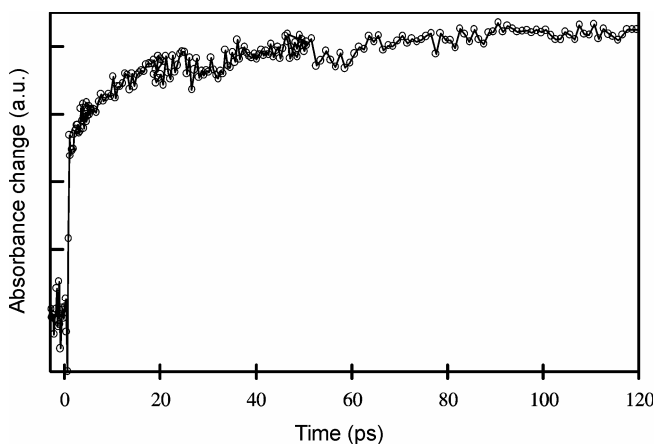
complexes, the slow component can be attributed to the vibrational cooling of the $^3$MLCT state[47–49]. A combined study by picosecond time-resolved Raman and absorption spectroscopy showed that the growth of the transient absorption is linked to the thermalization of the $^3$MLCT state[50]. The higher extinction coefficient of the thermalized $^3$MLCT compared to the hot $^3$MLCT can be attributed to an increase in the electronic transition moment and/or the vibrational overlap during the vibrational cooling[50]. The vibrational cooling times measured here in the ruthenium terpyridine complex are in line with recent femtosecond data on metal polypyridine complexes[51].

### Forward electron transfer

In order to determine the electron transfer rates from the Ru terpyridine complex into the TiO$_2$, we simultaneously monitor the decay of the dye excited state and the formation of the oxidized state with the probe wavelength at 570 nm. As shown in Figure 3, a large extinction coefficient changes is expected at this probe wavelength due to the different spectral signature of $P_0^*$ and $P_0^+$.

Figure 5 shows the transient absorption data obtained for the $P_0$, $P_1$ and $P_2$ systems. The signal recorded at 570 nm for the three systems exhibits a rise within the instrument response, which is attributed to the formation of the hot $^3$MLCT state. The decay of the signal recorded at 570 nm reflects simultaneously the decay of the hot $^3$MLCT state and the formation of the dye oxidized state (eq. (2)). Transient absorption data for the three systems can be well fitted with a bi-exponential function convoluted with a Gaussian instrument response giving the following time constants and amplitudes (in parentheses): 850 fs (48%) and 16 ps (52%) for $P_0$, 1.8 ps (39%) and 72 ps (61%) for $P_1$ and 3.7 ps (60%) and 51 ps (40%) for $P_2$.
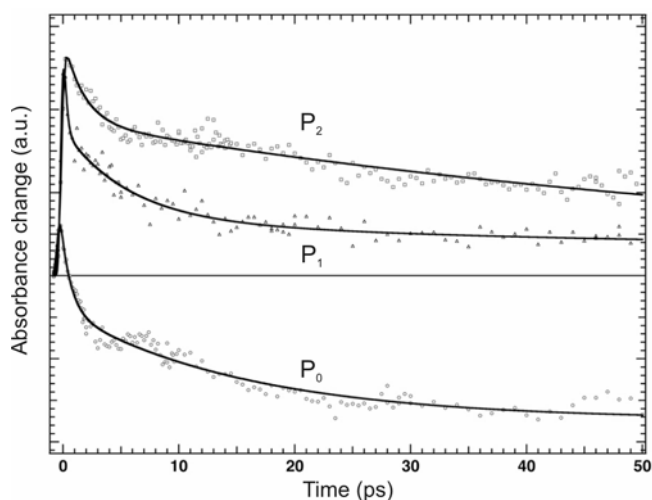


**Figure 4.** Transient absorption data of the donor $P_0$ (($C_4H_9$)$_4$N[2,2′ : 6′,2″-terpyridine-4′-phosphonate(NCS)$_3$Ru]) in ethanolic solution. Pump and probe wavelengths at 530 and 570 nm respectively. Data obtained in 1 mm path length quartz cuvette.



**Figure 5.** Femtosecond transient absorption data in $P_0$ (circles), $P_1$ (triangles) and $P_2$ (squares) systems recorded at 570 nm after pumping at 535 nm.

## Back electron transfer

The dynamics of the back electron transfer (BET) (eq. (3)) between the injected electrons and the oxidized dyes has been studied by flash photolysis by probing at 680 nm. Figure 6 shows the transient absorption data obtained for the $P_0$, $P_1$ and $P_2$ systems. The traces exhibit rise within the laser pulse duration (5 ns), reflecting the oxidized dye formation, followed by a slow recovery, which corresponds to the BET process (eq. (3)). In order
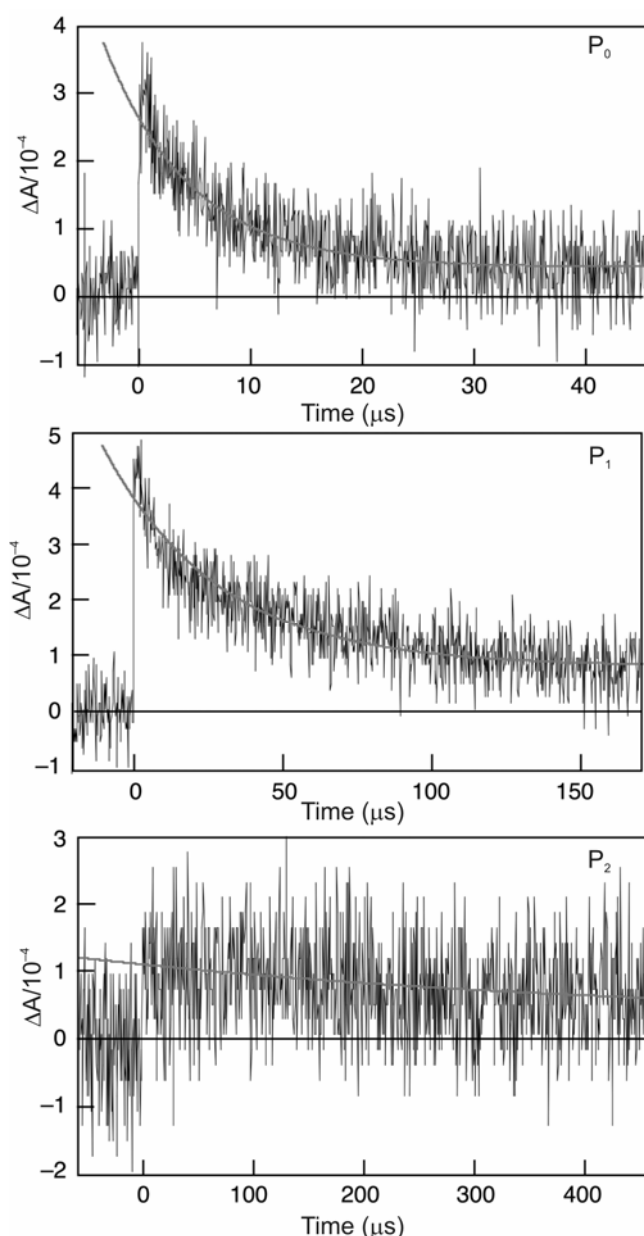


**Figure 6.** Transient absorbance decay kinetics of the oxidized states of $P_0$, $P_1$ and $P_2$ dyes adsorbed on nanocrystalline TiO$_2$. Absorbance changes were measured at a probe wavelength of 680 nm upon 600 nm pulsed laser excitation (5 ns FWHM pulse duration, 40 μJ/cm$^{-2}$ pulse fluence, 30 Hz repetition rate). Signals shown were obtained by typically averaging over 2000 laser shots.

to compare the three different systems within the same conditions, the measurements were performed at very low light excitation intensity. Within this regime, less than one electron per TiO$_2$ nanoparticle on an average is injected and the recombination rate constants are independent of light intensity. This method allows a clear comparison of the ET rates among the three systems. Under these conditions, the traces recorded at 680 nm are well fitted with a single exponential decay. This approach avoids complex kinetics arising from nonlinear effects. Moreover, trapping and detrapping processes, which can alter the distance dependence, are also avoided within this regime. Data obtained for the forward and the back ET rates for the three systems are summarized in Table 1.

## Distance dependence of electron transfer rates

For the forward electron transfer, the distance corresponds to the spatial separation between the $\pi^*$ orbital of the terpyridyl ligand and the nearest Ti$^{4+}$ of the TiO$_2$ surface. These distances in $P_0$, $P_1$ and $P_2$, D–B–A systems were calculated from semi-empirical geometry optimization (ZINDO) carried out with the CAChe software package assuming that ET occurs through the phenylene bridges. The distances between the donor and the acceptor are 9, 13.4 and 17.8 Å in $P_0$, $P_1$ and $P_2$ systems respectively. In general, the distance dependence of ET rates in D–B–A systems is described by (eq. (4)) (refs 52 and 53). In this expression, $\beta$ corresponds to the so-called damping factor of the ET rate, $k_0$ is the ET rate constant at the contact distance and $d$ the distance between the donor and the acceptor.

$$k_{ET} = k_0 \exp(-\beta d). \tag{4}$$

Figure 7 presents the semi-log plot of the forward ET rates as a function of the distance. The slope of the semi-log plot of the fast component of the FET rates gives a damping factor value $\beta$ of $0.16 \pm 0.02$ Å$^{-1}$. The slow component, which arises from adsorbed molecules in the aggregates forms[37], does not exhibit a clear trend in the FET dynamics. The amplitudes of the rate constants are comparable in $P_0$ and $P_1$ and slightly different in $P_2$ system. The plot of the average rate of FET as a function of the distance gives a $\beta$ value of $0.13 \pm 0.05$ Å$^{-1}$. For BET, a damping factor value of $0.47 \pm 0.05$ Å$^{-1}$ is obtained from the slope of the plot shown in Figure 8.

**Table 1.** Time constants for the FET and the BET in $P_0$, $P_1$ and $P_2$ systems adsorbed on nanocrystalline TiO$_2$

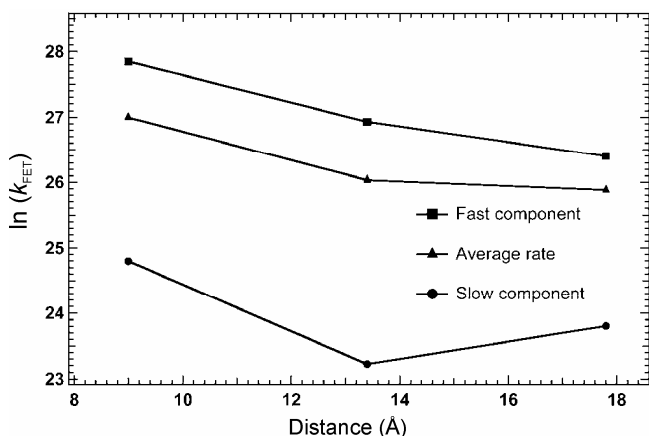| Distance (Å) | FET time constants (ps) and weight (in brackets) | BET time constants (μs) |
|---|---|---|
| 9 | 0.85 (48%) and 16 (52%) | 7.7 |
| 13.4 | 1.8 (39%) and 72 (61%) | 42 |
| 17.8 | 3.7 (60%) and 51 (40%) | 476 |

**Figure 7.** Semi-log plot of the forward electron transfer the rate constants as a function of the distance between the donor and the acceptor.
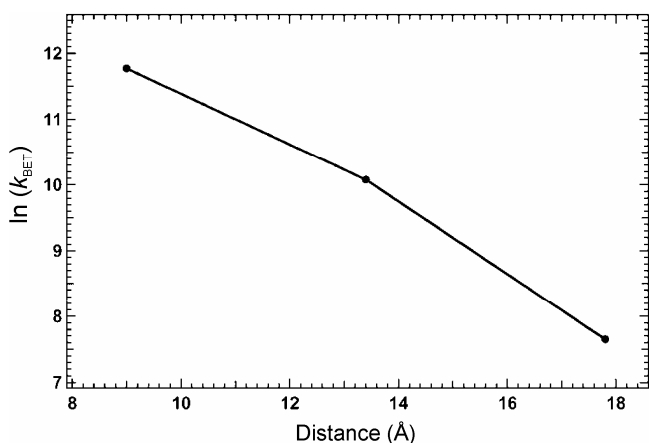


**Figure 8.** Semi-log plot of the backward electron transfer the rate constants as a function of the distance between the donor and the acceptor.

## Discussions

The main findings of the present study can be summarized as follows: (i) the relaxation of the nonequilibrium vibrations of the $^3$MLCT Ru terpyridine complex donor takes place in 12 ps in solution; (ii) a sharp difference in the damping factor values is observed (0.16 Å$^{-1}$ for FET versus 0.47 Å$^{-1}$ for BET); (iii) the damping factor for FET is the lowest reported so far for $p$-oligo(phenylene) bridges; (iv) FET takes place on an ultrafast time scale, about six orders of magnitude faster than BET and (v) the forward ET occurs far from equilibrium during the relaxation of the donor nonequilibrium vibrations as previously observed[35,38,41–43].

Damping factor values of $\beta = 0.5 \pm 0.1$ Å$^{-1}$ in $p$-oligo(phenylene) bridges obtained by current measurements with self-assembled monolayers are reported earlier[17–19,23]. In addition, beta values of 0.4, 0.65 and 0.46–0.67 Å$^{-1}$ are reported in molecular D–B–A systems with zinc porphyrin[20], ruthenium polypyridine[22] and phe-

nothiazine[21] as the donors respectively. Thus, the beta value found here for BET lies in the range of the previously reported values. Photoinduced electron transfer rates have also been reported in conjugated and non-conjugated rigid-rod bridges anchored to TiO$_2$ acceptors[54–57]. However, to the best of our knowledge, charge transfer properties of rigid molecular bridges linked to a semiconductor as the acceptor are poorly documented. Myahkostupov *et al.*[31] reported an ultrafast ET and a low damping factor ($\beta = 0.04$ Å$^{-1}$) with an OPE bridge and TiO$_2$ nanoparticles as the acceptor.

ET rate from a donor to an acceptor can be written as follows.

$$k_{ET} = \frac{2\pi}{\eta} |H_{DA}|^2 FC, \tag{5}$$

where H$_{DA}$ is the electronic coupling between the donor and the acceptor and FC the Franck–Condon weighted density of states factor that contains the driving force ($\Delta G$) and the reorganization energy $\lambda$.

Intuitively, the exponential decay of ET rate is often attributed to the exponential decay of the electronic coupling (decrease of the overlap between the donor and the acceptor orbitals)[52,53]. Therefore, eq. (5) can be simplified to eq. (6) where $H_0$ is the electronic coupling at the contact distance. The contribution of $\Delta G$ and $\lambda$ on the distance dependence of ET rate is small when the donor–acceptor distance is larger than 10 Å (refs 58 and 59).

$$|H_{DA}|^2 = |H_0|^2 \exp(-\beta d). \tag{6}$$

In the present D–B–A system, the Franck–Condon factor can be neglected since the electronic coupling is the main factor that governs ET rate from a dye excited into the conduction band[33]. Finally, the Marcus description assumes that the vibrations of the donor are in a thermal equilibrium on the time scale of the ET transfer process[58]. This is not the case for the forward ET since the donor is in a highly vibrationally excited state during the ET process.

As shown in Figures 7 and 8, the extrapolation to the contact distance indicates that the electronic coupling at the contact distance for FET ($H_{0(FET)}$) is much larger than for BET ($H_{0(BET)}$). Different $H_0$ values are expected since different orbitals are involved in FET with respect to BET. Basically, in the FET process the electronic coupling corresponds to the overlap between the 3d orbitals of the surface titanium atom and the $\pi$ orbital of the terpyridine ligand. In contrast, BET consists of a charge transfer from a trapped electron onto the TiO$_2$ surface towards the highest occupied molecular orbitals (HOMO) of the donor, which are shared by Ru(III) and the SCN ligands. However, using eq. (6), the damping factor beta is independent from $H_0$ and so from the orbitals, since the damping factor is obtained from the slope[60]. Thus, the different

beta values do not originate from the different orbitals involved in FET and BET processes.

The unusual low damping factor value for FET may be explained by a partial delocalization of the lowest unoccupied molecular orbitals (LUMO) of the Ru ter-pyridine sensitizer along the phenylene bridge. This would reduce the distance between the donor and the acceptor leading to a low beta value. However, the comparable electronic absorption spectra of $P_0$, $P_1$ and $P_2$ do not provide indications of an electronic delocalization through the molecular bridge.

The different beta values obtained for FET and BET suggest that the damping factor is not only sensitive to the molecular bridge but to the full D–B–A system[61,62]. In fact, it was observed that the beta value is also dependent on the donor–bridge energetics[59,60]. The relation between the energetics of the donor/bridge interface and the damping factor can be formulated within the McConnel model[64] by

$$\beta = \frac{2}{R_0} \ln \left| \frac{\Delta E}{H_B} \right|. \tag{7}$$

Here $\Delta E$ is the tunnelling energy gap, $H_B$ the electronic coupling between adjacent molecules in the bridge and $R_0$ the length of a bridge unit $a$. Only the energy gap $\Delta E$ is related to the energetics of the donor/bridge interface, the two other parameters are specific to the molecular bridge. Recently, experimental and theoretical investigations have shown that the damping factor is indeed dependent of the energy gap according to the McConnel model[61–63]. Within a simple picture, the electron transfer in a D–B–A system can be seen as an electron moving from the LUMO (or higher states) of the donor through the LUMO (or higher states) of the bridge to be injected into the quasi-continuum of empty electronic states of the TiO$_2$ conduction band. Basically, the tunnelling energy gap $\Delta E$ can be defined as $\Delta E = E_{LUMO}(\text{bridge}) - E_{LUMO}(\text{donor})$. However, it is difficult to estimate $\Delta E$ of the present D–B–A system because the electron transfer occurs under nonequilibrium conditions. Indeed, in the present heterogeneous D–B–A system, there is a temporal overlap between the ET process and the relaxation of the non-equilibrium vibrations. The different subsystems, the donor, the bridge and the acceptor are not in thermal equilibrium and the full D–B–A system cannot be described by means of a statistical distribution. The non-equilibrium vibrations at the donor–bridge interface strongly perturb the tunnelling energy gap, may bring the donor and the bridge states into resonance or may lead to the formation of electronic states in the energy-gap by vibronic coupling[65]. We note that the damping factors of p-oligo(phenylene) bridges reported for homogeneous D–B–A systems were obtained at thermal equilibrium[20–22]. Here, in contrast to homogeneous D–B–A systems, the presence of an excess energy strongly affects the ET

process as described here. The donor is photoexcited at the blue side of the MLCT band with a photon energy of 2.3 eV. The electronic transition induced by the femto-second laser pulse involves the promotion of an electron from the Ru(II) d$\pi$ orbital to the $\pi^*$ orbital of the terpyridine ligand with an excess energy of about 0.3 eV (refs 66–68). The excess of photonic energy injected into the donor is deposited in the vibrational modes coupled to the photoinduced electronic transition. This generates a population of nonequilibrium vibrations in the terpyridine ligand with candidates as the accepting modes at 1600, 1468 and 1413 cm$^{-1}$ (ref. 69). Our femtosecond data on the dynamics of the donor excited state indicates that the lifetime of these nonequilibrum vibrations is as long as 12 ps in solution.

To fully account for the unusual low damping factor for FET, inclusion of the population of nonequilibrium vibrations of the donor is necessary because strong electron/vibration couplings exist in the present D–B–A system. Indeed, calculations[70] confirmed by inelastic electron tunnelling spectroscopy[71] indicate that the $\nu(8a)$ and $\nu(18a)$ stretching modes at 1140 and 1580 cm$^{-1}$ of the biphenyl, according to Varsayni nomenclature[72], are strongly coupled to the tunnelling electrons. The main vibrational modes observed in the FT–IR spectrum of the donor–bridge $P_2$ located at 1600 and 1135 cm$^{-1}$ correspond to the vibrational modes that are strongly coupled to tunnelling electrons.

The charge transfer through molecular bridges has been studied within a Green function formalism[73]. It can be shown that the behaviour of the tunnelling electron evolves from a free-electron-like to a polaron-like when the system enters the regime wherein the vibrational cooling and the charge transfer times are comparable[73]. This is accompanied by a change in the tunnelling energy gap[73–75]. In addition, quantum versions of the Su–Schriffer–Heeger (SSH) model[74] predict that the coupling between tunnelling electrons and vibrations induces a decrease of the energy gap, which is associated with the formation of a virtual polaron[75,76]. According to eq. (7) a decrease of the energy gap lowers the damping factor.

In brief, our results in accordance with theory suggest that the low beta value is due to the transport of a non-equilibrium polaron, which induces a decrease of the tunnelling energy gap. A nonequilibrium polaron can be envisioned as a photoexcited electron accompanied by its own nonequilibrium vibration initiated during the photoinduced electronic transition. This nonequilibrium polaron is a transient particle since an ultrafast thermalization occurs to dissipate the excess energy in order to reach a stationary regime, i.e. a self-trapped electron onto the TiO$_2$ surface. The motion of a nonequilibrium polaron is thus not slowed down compared to the free tunnelling electron since it occurs in a dissipative system far from equilibrium. Indeed, the dynamics of the nonequilibrium polaron is expected to be governed by the rate of the intra-

molecular vibrational redistribution (IVR) within the D–B–A system. The rate of excess vibrational energy dissipation of the D–B system toward the TiO$_2$ surface (excitation of phonons) plays a crucial role on the lifetime of the nonequilibrium polaron. Unfortunately, the rate of vibrational energy transfer of metal polypyridyl complexes toward a metal oxide surface remains unknown. To set a time scale, the vibrational energy flow from the 1510 cm$^{-1}$ mode toward the 860 cm$^{-1}$ mode occurs within 4 ps in a aromatic derivative (p-nitro aniline and betaine)[77,78]. This is comparable to the FET rate measured here in the $P_2$ system. At least two conditions must be fulfilled to observe the enhancement of the electron transmission due to the transport of a nonequilibrium polaron: (i) the ET rate must be comparable to the nonequilibrium vibrational relaxation rate and (ii) a coupling between the photoexcited electron and the vibrational modes must exist in the D–B–A system. The use of TiO$_2$ as acceptor in D–B–A systems with molecular bridges wherein vibronic couplings exist (for example, OPE)[71] may fulfil these conditions[30].

## Conclusions

We have measured by transient absorption spectroscopy both the forward and the back ET in the same D–B–A systems. We observed a dramatic difference in the time scales between FET and BET as well as for the damping factors. FET occurs in the femto-picosecond regime with a beta value of 0·16 Å$^{-1}$ whereas the BET takes place in the micro-millisecond regime with a beta value of 0.47 Å$^{-1}$. These results confirm that the damping factor is not only dependent on the nature of the molecular bridge but to the full D–B–A system as previously reported[59–62]. The unusual low beta value obtained for FET is linked to the specific properties of the present D–B–A system, i.e. the occurrence of ET during the nonequilibrium vibrational relaxation of the donor. The nonequilibium vibrations at the donor/bridge interface induce a decrease of the tunnelling energy gap and thus an unusual low beta value. In other terms, FET and the vibrational energy flow occur in a synchronized cooperative way (nonequilibrium polaron). On the basis of vibrational spectra of $P_0$, $P_1$ and $P_2$ and the vibronic coupling in p-oligo(phenylene) bridges, we propose that the nonequilibrium polaron is formed by the photoexcited electron accompanied by the high-frequency longitudinal nonequilibrium mode at 1600 cm$^{-1}$. In the present system, the excess energy can be harnessed in a nonequilibrium nonlinear process to achieve an efficient energy flow along a molecular chain. The TiO$_2$ as the acceptor in this heterogeneous D–B–A system fills up different roles: (i) the high density of empty electronic states of the TiO$_2$ conduction band leads to a giant electronic coupling at the contact distance $H_0$; (ii) this high $H_0$ value brings the heterogeneous D–B–A

system into a regime wherein the entanglement between the dynamics of the tunnelling electron and the nonequilibrium vibrations become possible and (iii) new channels of vibrational energy dissipation from the D–B systems with the excitation of surface TiO$_2$ phonons are open. We speculate that rich physics can be observed by using such heterogeneous D–B–A systems, in which the propagation of polarons, solitons, breathers could be observed in real-time by combining ultrafast vibrational and UV–Vis spectroscopy. Such studies are currently in progress.

Supporting Information available online.

1. Gray, H. B. and Winkler, J. R., Electron transfer in proteins. *Annu. Rev. Biochem.*, 1996, **65**, 537.
2. Moser, C. C., Page, C. C., Farid, R. and Dutton, P. L., Biological electron transfer. *J. Bioenerg. Biomembr.*, 1995, **27**, 263–274.
3. Franzen, S., Goldstein, R. F. and Boxer, S. G., Distance dependence of electron-transfer reactions in organized systems: the role of superexchange and non-Condon effects in photosynthetic reaction centers. *J. Phys. Chem.*, 1993, **97**, 3040–3053.
4. Holmlin, R. E., Danliker, P. J. and Barton, J. K., Charge Transfer through the DNA base stack. *Angew. Chem. Int. Ed. Engl.*, 1997, **36**, 2714–2730.
5. Meade, T. J. and Kayyem, J. F., Electron transfer through DNA. *Angew. Chem. Int. Ed. Engl.*, 1995, **34**, 352.
6. Daizadeh, I., Medvedev, E. S. and Stuchebrukhov, A. A., Effect of protein dynamics on biological electron transfer. *Proc. Natl. Acad. Sci. USA*, 1997, **94**, 3703.
7. Wan, C., Fiebig, T., Kelley, S. O., Treadway, C. R., Barton, J. K. and Zewail, A. H., Femtosecond dynamics of DNA-mediated electron transfer. *Proc. Natl. Acad. Sci. USA*, 1999, **96**, 6014.
8. Fiebig, T., Wan, C., Kelley, S. O., Barton, J. K. and Zewail, A. H., Femtosecond dynamics of the DNA intercalator ethidium and electron transfer with mononucleotides in water. *Proc. Natl. Acad. Sci. USA*, 1999, **96**, 1187.
9. Schuster, G. B., Long-range charge transfer in DNA: transient structural distortions control the distance dependence. *Acc. Chem. Res.*, 2000, **33**, 253–260.
10. Gray, H. B. and Winkler, J. R., Long-range electron transfer. *Proc. Natl. Acad. Sci. USA*, 2005, **102**, 3534–3539.
11. Nitzan, A. and Ratner, M. A., Electron transport in molecular wire junctions. *Science*, 2003, **300**, 1384.
12. Zhu, X.-Y., Charge transport at metal−molecule interfaces: a spectroscopic view. *J. Phys. Chem. B*, 2004, **108**, 8778.
13. Joachim, C., Gimzewski, J. K. and Aviram, A., Electronics using hybrid-molecular and mono-molecular devices. *Nature*, 2000, **408**, 541.
14. Grätzel, M. and Moser, J.-E., *Electron Transfer in Chemistry* (eds Balzani, V. and Gould, I. R.), Wiley-VCH, New York, 2001, vol. 5, pp. 589–644.
15. Moser, J.-E., Solar cells: later rather than sooner. *Nat. Mat.*, 2005, **4**, 723.
16. Moser, J.-E., Bonhôte, P. and Grätzel, M., Molecular photovoltaics. *Coord. Chem. Rev.*, 1998, **171**, 245–250.
17. Fan, F.-R. F. *et al.*, Charge transport through self-assembled monolayers of compounds of interest in molecular electronics. *J. Am. Chem. Soc.*, 2002, **124**, 5550.
18. Wold, D. J., Haag, R., Rampi, M. A. and Frisbie, C. D., Distance dependence of electron tunneling through self-assembled monolayers measured by conducting probe atomic force microscopy: unsaturated versus saturated molecular junctions. *J. Phys. Chem. B*, 2002, **106**, 2813–2816.

19. Holmlin, R. E. *et al.*, Electron transport through thin organic films in metal−insulator−metal junctions based on self-assembled monolayers. *J. Am. Chem. Soc.*, 2001, **123**, 5075–5085.

20. Helms, A., Heiler, D. and McLendon, G., Electron transfer in bis-porphyrin donor–acceptor compounds with polyphenylene spacers shows a weak distance dependence. *J. Am. Chem. Soc.*, 1992, **114**, 6227–6238.

21. Weiss, E. A., Ahrens, M. J., Sinks, L. E., Gusev, A. V., Ratner, M. A. and Wasielewski, M. R., Making a molecular wire: charge and spin transport through para-phenylene oligomers. *J. Am. Chem. Soc.*, 2004, **126**, 5577.

22. Indelli, M. T., Claudio, C., Flamigni, L., De Cola, L. and Scandola, F., Photoinduced electron transfer across oligo-*p*-phenylene bridges. Distance and conformational effects in Ru(II)−Rh(III) dyads. *Inorg. Chem.*, 2007, **46**, 5630–5641.

23. Venkataraman, L., Klare, J. E., Nuckolls, C., Hybertsen, M. S. and Steigerwald, M. L., Dependence of single-molecule junction conductance on molecular conformation. *Nature*, 2006, **442**, 904.

24. Nitzan, A., Electron transmission through molecules and molecular interfaces. *Annu. Rev. Phys. Chem.*, 2001, **52**, 681.

25. Asbury, J. B., Hao, E., Wang, Y. and Lian, T., Bridge length-dependent ultrafast electron transfer from Re polypyridyl complexes to nanocrystalline TiO₂ thin films studied by femtosecond infrared spectroscopy. *J. Phys. Chem. B*, 2000, **104**, 11957–11964.

26. Anderson, N. A., Ai, X., Chen, D., Mohler, D. L. and Lian, T., Bridge-assisted ultrafast interfacial electron transfer to nanocrystalline SnO₂ thin films. *J. Phys. Chem. B*, 2003, **107**, 14231–14239.

27. Anderson, N. A. and Lian, T., Ultrafast electron transfer at the molecule semiconductor nanoparticle interface. *Annu. Rev. Phys. Chem.*, 2005, **56**, 491–519.

28. Asbury, J. B., Hao, E., Wang, Y., Ghosh, H. N. and Lian, T., Ultrafast electron transfer dynamics from molecular adsorbates to semiconductor nanocrystalline thin films. *J. Phys. Chem. B*, 2001, **105**, 4545–4557.

29. Watson, D. F. and Meyer, G. J., Electron injection at dye-sensitized semiconductor electrodes. *Annu. Rev. Phys. Chem.*, 2005, **56**, 119–156.

30. Duncan, W. R. and Prezhdo, O. V., Theoretical studies of photoinduced electron transfer in dye-sensitized TiO₂. *Annu. Rev. Phys. Chem.*, 2007, **58**, 143–184.

31. Myahkostupov, M., Piotrowiak, P., Wang, D. and Galoppini, E., Ru(II)-Bpy complexes bound to nanocrystalline TiO₂ films through phenyleneethynylene (OPE) linkers: effect of the linkers length on electron injection rates. *J. Phys. Chem. C*, 2007, **111**, 2827–2829.

32. Bae, E. and Choi, W., Effect of the anchoring group (carboxylate vs phosphonate) in Ru-complex-sensitized TiO₂ on hydrogen production under visible light. *J. Phys. Chem. B*, 2006, **110**, 14792.

33. Miller, R. J. D., McLendon, G. L., Nozik, A., Schmickler, W. and Willig, F., *Surface Electron Transfer Processes*, VCH, New York, 1995, pp. 167–310.

34. Tachibana, Y., Grätzel, M., Moser, J. E., Klug, D. R. and Durrant, J. R., Subpicosecond interfacial charge separation in dye-sensitized nanocrystalline titanium dioxide films. *J. Phys. Chem.*, 1996, **100**, 20056.

35. Moser, J.-E. and Grätzel, M., Excitation wavelength dependence of photoinduced charge injection at the semiconductor-dye interface: evidence for electron transfer from vibrationally hot excited states. *Chimia*, 1998, **52**, 160.

36. Pelet, S., Grätzel, M. and Moser, J. E., Femtosecond dynamics of interfacial and intermolecular electron transfer at eosin-sensitized metal oxide nanoparticles. *J. Phys. Chem. B*, 2003, **107**, 3215–3224.

37. Wenger, B., Grätzel, M. and Moser, J.-E., Rationale for kinetic heterogeneity of ultrafast light-induced electron transfer from Ru(II) complex sensitizers to nanocrystalline TiO₂. *J. Am. Chem. Soc.*, 2005, **127**, 12150–12151.

38. Zimmermann, C., Willig, F., Ramakrishna, S., Burfeindt, B., Pettinger, B., Eichberger, R. and Storck, W., Experimental fingerprints of vibrational wave-packet motion during ultrafast heterogeneous electron transfer. *J. Phys. Chem. B*, 2001, **105**, 9245–9253.

39. Abuabara, S. G., Rego, L. G. C. and Batista, V. S., Influence of thermal fluctuations on interfacial electron transfer in functionalized TiO₂ semiconductors. *J. Am. Chem. Soc.*, 2005, **127**, 18234–18242.

40. Stier, W. and Prezhdo, O. V. J., Nonadiabatic molecular dynamics simulation of light-induced electron transfer from an anchored molecular electron donor to a semiconductor acceptor. *Phys. Chem. B*, 2002, **106**, 8047.

41. Rego, L. G. C. and Batista, V. S., Quantum dynamics simulations of interfacial electron transfer in sensitized TiO₂ semiconductors. *J. Am. Chem. Soc.*, 2003, **125**, 7989–7997.

42. Thoss, M., Kondov, I. and Wang, H., Theoretical study of ultrafast heterogeneous electron transfer reactions at dye–semiconductor interfaces. *Chem. Phys.*, 2004, **304**, 169.

43. Kondov, I., Wang, H. and Thoss, M., Theoretical study of ultrafast heterogeneous electron transfer reactions at dye–semiconductor interfaces: coumarin 343 at titanium oxide. *J. Phys. Chem. A*, 2006, **110**, 1364.

44. Amouyal, E., Mouallem-Babout, M. and Calzaferri, G., Excited states of M(II, d6)-4′-phenylterpyridine complexes: electron localization. *J. Phys. Chem.*, 1991, **95**, 7641.

45. Bauer, C., Boschloo, G., Mukhtar, E. and Hagfeldt, A., Interfacial electron-transfer dynamics in Ru(tcterpy)(NCS)₃-sensitized TiO₂ nanocrystalline solar cells. *J. Phys. Chem. B*, 2002, **106**, 12693.

46. McKusker, J. K., Femtosecond absorption spectroscopy of transition metal charge-transfer complexes. *Acc. Chem. Res.*, 2003, **36**, 876–887.

47. Damrauer, N. H. and McCusker, J. K., Ultrafast dynamics in the metal-to-ligand charge transfer excited-state evolution of [Ru(4,4′-diphenyl-2,2′-bipyridine)3]²⁺. *J. Phys. Chem. A*, 1999, **103**, 8440–8446.

48. Shaw, G. B., Styers-Barnett, D. J., Gannon, E. Z., Granger, J. C. and Papanikolas, J. M., Interligand electron transfer dynamics in [Os(bpy)3]²⁺: exploring the excited state potential surfaces with femtosecond spectroscopy. *J. Phys. Chem. A*, 2004, **108**, 4998–5006.

49. Henry, W. *et al.*, The early picosecond photophysics of Ru(II) polypyridyl complexes: a tale of two timescales. *J. Phys. Chem. A*, 2008, **112**, 4537–4544.

50. Liard, D. J., Busby, M., Matousek, P., Towrie, M. and Vlcek Jr, A., Picosecond relaxation of 3MLCT excited states of [Re(Etpy)(CO)3(dmb)]+ and [Re(Cl)(CO)3(bpy)] as revealed by time-resolved resonance Raman, UV−vis, and IR absorption spectroscopy. *J. Phys. Chem. A*, 2004, **108**, 2363–2369.

51. Henry, W. *et al.*, Addition/correction. The early picosecond photophysics of Ru(II) polypyridyl complexes: a tale of two timescale. *J. Phys. Chem. A*, 2008, **112**, 10704.

52. Barbara, P. F., Meyer, T. J. and Ratner, M. A., Contemporary issues in electron transfer research. *J. Phys. Chem.*, 1996, **100**, 13148.

53. Adams, D. M. *et al.*, Charge transfer on the nanoscale: current status. *J. Phys. Chem. B*, 2003, **107**, 6668.

54. Galoppini, E., Guo, W., Zhang, W., Hoertz, P. G., Qu, P. and Meyer, G. J., Long-range electron transfer across molecule−nanocrystalline semiconductor interfaces using tripodal sensitizers. *J. Am. Chem. Soc.*, 2002, **124**, 7801–7811.

55. Galoppini, E., Guo, W., Qu, P. and Meyer, G. J., Long-distance electron transfer across molecule−nanocrystalline semiconductor interfaces. *J. Am. Chem. Soc.*, 2001, **123**, 4342–4343.

56. Hoertz, P. G., Carlisle, R. A., Meyer, G. J., Wang, D., Piotrowiak, P. and Galoppini, E., Organic rigid-rod linkers for coupling chromophores to metal oxide nanoparticles. *Nano Lett.*, 2003, **3**, 325–330.

57. Wang, D., Mendelsohn, R., Galoppini, E., Hoertz, P. G., Carlisle, R. A. and Meyer, G. J., Excited state electron transfer from Ru(II) polypyridyl complexes anchored to nanocrystalline TiO$_2$ through rigid-rod linkers. *J. Phys. Chem. B*, 2004, **108**, 16642–16653.

58. Marcus, R. A., On the theory of oxidation–reduction reactions involving electron transfer. *J. Chem. Phys.*, 1956, **24**, 966.

59. Davis, W. B., Walter, A. S., Ratner, M. A. and Wasielewski, M. R., Molecular-wire behaviour in *p*-phenylenevinylene oligomers. *Nature*, 1998, **396**, 60.

60. Lewis, F. D., Liu, J., Weigel, W., Rettig, W., Kurnikov, I. V. and Beratan, D. N., *Proc. Natl. Acad. Sci. USA*, 2002, **99**, 12536–12541.

61. Wiberg, J., Guo, L., Pettersson, K., Nilsson, D., Ljungdahl, T., Mårtensson J. and Albinsson, B., Charge recombination versus charge separation in donor–bridge–acceptor systems. *J. Am. Chem. Soc.*, 2007, **129**, 155–163.

62. Albinsson, B. and Mårtensson, J., Long-range electron and excitation energy transfer in donor–bridge–acceptor systems. *J. Photochem. Photobiol. C*, 2008, **9**, 138–155.

63. Pettersson, K., Kyrychenko, A., Rnnow, E., Ljungdahl, T., Mårtensson, J. and Albinsson, B., Singlet energy transfer in porphyrin-based donor–bridge–acceptor systems: interaction between bridge length and bridge energy. *J. Phys. Chem. A*, 2006, **110**, 310–318.

64. McConnel, H., Intramolecular charge transfer in aromatic free radicals. *J. Chem. Phys.*, 1961, **35**, 508.

65. Heeger, A. J., Nobel lecture: semiconducting and metallic polymers: the fourth generation of polymeric materials. *Rev. Mod. Phys.*, 2001, **73**, 681.

66. Nazeeruddin, M. K. *et al.*, Engineering of efficient panchromatic sensitizers for nanocrystalline TiO$_2$-based solar cells. *J. Am. Chem. Soc.*, 2001, **123**, 1613–1624.

67. Nazeeruddin, M. K., Zakeeruddin, S. M., Humphry-Baker, R., Kaden, T. A. and Grätzel, M., Determination of pKa values of 4-phosphonato-2,2′ : 6′,2″-terpyridine and its ruthenium(II)-based photosensitizer by NMR, potentiometric and spectrophotometric methods. *Inorg. Chem.*, 2000, **39**, 4542–4547.

68. Zakeeruddin, S. M. *et al.*, Molecular engineering of photosensitizers for nanocrystalline solar cells: synthesis and characterization of Ru dyes based on phosphonated terpyridines. *Inorg. Chem.*, 1997, **36**, 5937–5946.

69. Schoonover, J. R. and Strouse, G. F., Time-resolved vibrational spectroscopy of electronically excited inorganic complexes in solution. *Chem. Rev.*, 1998, **98**, 1335–1355.

70. Troisi, A., Ratner, M. and Nitzan, A., Vibronic effects in off-resonant molecular wire conduction. *J. Chem. Phys.*, 2003, **118**, 6072.

71. Kushmerick, J. G., Lazorcik, J., Patterson, C. H., Shashidhar, R., Seferos, D. S. and Bazan, G. C., Vibronic contributions to charge transport across molecular junctions. *Nano Lett.*, 2004, **4**, 639–642.

72. Varsanyi, G., *Vibrational Spectra of Aromatic Derivatives*, Academic, New York, 1969.

73. Yu, Z. G., Smith, D. L., Saxena, A. and Bishop, A. R., Green's function approach for a dynamical study of transport in metal/organic/metal structures. *Phys. Rev. B*, 1999, **59**, 16001.

74. Heeger, A. J., Kivelson, S., Schrieffer, J. R. and Su, W.-P., Solitons in conducting polymers. *Rev. Mod. Phys.*, 1988, **60**, 781.

75. Ness, H., Shevlin, S. A. and Fisher, A. J., Coherent electron–phonon coupling and polaron-like transport in molecular wires. *Phys. Rev. B*, 2001, **63**, 125422.

76. Ness, H. and Fisher, A. J., Quantum inelastic conductance through molecular wires. *Phys. Rev. Lett.*, 1999, **83**, 452.

77. Kosich, V., Wernecke, W., Dreyer, J., Brzekinka, K.-W., Rini, M., Kummrow, A. and Elsaesser, T., Vibrational excitation and energy redistribution after ultrafast internal conversion in 4-nitroaniline. *J. Chem. Phys.*, 2002, **117**, 719.

78. Niberring, E. T. J., Fidder, H. and Pines, E., Utrafast chemistry: using time-resolved vibrational spectroscopy for interrogation of structural dynamics. *Annu. Rev. Phys. Chem.*, 2005, **56**, 337.

79. Hogiu, S., Werncke, W., Pfeiffer, M., Dreyer, J. and Elsaesser, T., Mode-specific vibrational excitation and energy redistribution after ultrafast intramolecular electron transfer. *J. Chem. Phys.*, 2000, **113**, 1587.